Degradation State Identification for Hydraulic Pumps Based on Multi-scale Ternary Dynamic Analysis, NSGA-II and SVM

Mochao Pei, Hongru Li, He Yu

Army Engineering University, Shijiazhuang 050003, China
Correspondence to: Hongru Li/ lihr168@sohu.com

Degradation state identification for hydraulic pumps is crucial to ensure system performance. As an important step, feature extraction has always been challenging. The non-stationary and non-Gaussian characteristics of the vibration signal are likely to weaken the performance of traditional features. In this paper, an efficient feature extraction algorithm named multi-scale ternary dynamic analysis (MTDA) is proposed. MTDA reconstructs the phase space based on the given signal and converts each embedding vector into a ternary pattern independently, which enhances its capacity of describing the details of non-stationary signals. State entropy (SE) and state transition entropy (STE) are calculated to estimate the dynamical changes and complexity of each signal sample. The excellent performance of SE and STE in detecting frequency changes, amplitude changes, and the development process of fault is verified with the use of four simulated signals. The proposed multi-scale analysis enables them to provide a more precise estimation of entropy. Furthermore, support vector machine (SVM) and nondominated sorting genetic algorithm II (NSGA-II) are introduced to conduct feature selection and state identification. NSGA-II and SVM can conduct the joint optimization of these two goals. The details of the method proposed in this paper are tested using simulated signals and experimental data, and some studies related to the fault diagnosis of rotating machinery are compared with our method. All the results show that our proposed method has better performance, which obtains higher recognition accuracy and lower feature set dimension.

Keywords: Multi-scale ternary dynamic analysis(MTDA), NSGA-II and SVM, Hydraulic pump, Degradation state identification.

1. INTRODUCTION

It is well-known that the application of hydraulic systems can be found in many fields such as engineering machinery, metallurgy, transportation, aeronautics and astronautics [1]. As a component for transferring and converting energy, the hydraulic pump plays a key role in hydraulic systems. Many terrible safety accidents and economic losses are attributed to the failure of the hydraulic pump and the resulting paralysis of the hydraulic system [2]. Therefore, monitoring the degradation state of hydraulic pumps and implementing effective measures are conducive to the long-term and reliable operation of the system. As an important component of Prognostic and Health Management (PHM), degradation state identification has received extensive attentions in various areas [3]. The performance and reliability of hydraulic pumps have an urgent need of high-precision degradation state identification [4].

Nowadays, increasing attention has been paid to equipment condition monitoring and fault prognosis with vibration analysis methods. In some cases, the abnormal states of the equipment such as cavitation in pumps can be detected by analyzing the vibration signals [5]. The vibration signal obtained from the acceleration sensor is also widely used in condition monitoring for hydraulic pumps due to its fast

reactivity and bundant state information [6]. In general, the use of vibration signals for condition monitoring and fault prognosis consists of four steps, data acquisition and analysis, feature extraction and screening, model construction, training and validation, pattern recognition, and prognosis [7]. As crucial steps, feature extraction and selection are directly related to the accuracy and timeliness of degradation state identification.

Over the past few years, the traditional features of time-domain, frequency-domain and time-frequency domain had been applied to fault diagnosis of mechanical equipment [8]. M. M. Tahir et al. [9] extracted some time-domain statistical features in their study: variance, mean values, skewness, crest factor, etc. SVM, Decision tree, and Bayesian network (BN) were all used to diagnose bearing faults. Ziwei Wang et al. [10] proposed a novel approach of a random forest classifier for fault diagnosis in rolling bearings. The wavelet packet decomposition was applied for fault feature extraction. Yonggang Xu et al. [11] proposed empirical scanning spectrum kurtosis (ESSK) for fault feature extraction of rolling element bearings. Xiaoan Yan et al. [12] used variational modal decomposition, fast Fourier transform, and statistical analysis to extract the fault features of rolling bearings in their study. SVM was used for fault condition

identification of rolling bearings, whose parameters were optimized by the particle swarm optimization algorithm.

However, the faults of hydraulic systems are not as obvious and straightforward as common electromechanical structures, which makes it challenging to obtain degradation features [13]. In the process of hydraulic pump operation, vibration signals show prominent nonlinear and non-Gaussian characteristics due to the influence of fluid compressibility, fluid-structure coupling between pump source and servo system, and inherent mechanical vibration, which will lead to a remarkable decrease in the sensitivity of many traditional time-domain features [14]. Due to the interference of intense noise, the capability of traditional frequency domain and time-frequency domain features will also be weakened to some extent. Hence, a more effective method for feature extraction and degradation state identification of hydraulic pumps has become an urgent task.

In recent years, some researchers have shown an increasing interest in applying information theory, symbolic dynamic theory, variants of the texture analysis technique and deep learning to fault diagnosis [15]-[17]. The application of these novel methods overcomes the shortcomings of traditional methods to a certain extent. Yukui Wang et al. [18] proposed spatial information entropy and applied it to the degradation state identification of hydraulic pumps. Zhenghong Wu et al. [19] proposed an adaptive deep transfer learning for bearing fault diagnosis. Yongbo Li et al. [20] proposed a new dynamical indicator called modified multi-scale symbolic dynamic entropy (MMSDE). It combined the merits of symbolic dynamic filtering and information theory. It was experimentally demonstrated to have better fault detection capacity than modified multi-scale sample entropy (MMSE) and modified multi-scale permutation entropy (MMPE). Magda Ruiz et al. [21] converted the one-dimensional time series obtained from the wind turbine into a two-dimensional matrix and transformed the matrix into a grayscale image. Finally, texture features were obtained from grayscale images. This method inspired us to apply texture analysis techniques to degradation feature extraction. Recently, Melih Kuncan et al. [22] developed a method called one-dimensional local ternary pattern (1D-TP) to extract the fault features of rolling bearings. Yılmaz Kaya et al. [23] proposed a novel feature extraction method based on co-occurrence matrices for bearing vibration signals. The aforementioned Melih Kuncan, Yılmaz Kaya et al. have been committed to applying the modified texture analysis to bearing fault diagnosis in recent years, and many enlightening results have been proposed [24]-[26]. The texture analysis or its variants are simple and effective, which provide stable features for fault diagnosis. The Operators such as Local Binary Pattern (LBP) [26] and 1D-TP compare the pixel (or amplitude) of the center point with those of the surrounding points, thus they are local feature descriptors, which are suitable for non-stationary signals.

While some of the feature extraction methods applied previously have their advantages, their comprehensive capacity to reflect the deterioration of equipment performance still needs to be improved. First, deep learning requires a large number of data samples to obtain good recognition results. Second, in the field of fault diagnosis, a fault sample is likely to contain a small number of data points, which makes a one-dimensional signal into a small-size image. Consequently, the performance of texture analysis may be limited in this case. For this reason, variants of texture analysis such as 1D-TP seem to be more suitable for samples with a small number of data points. However, texture analysis and its variants produce large-scale feature sets, which will bring some troubles when subsequent operations such as feature selection and fusion are conducted. Anyway, a small-size feature set is our goal. Furthermore, the features provided by texture analysis and its variants cannot describe the dynamic changes of vibration signals. Third, entropy is effective in detecting the dynamic characteristics of signals. However, as we will prove later in this paper, some entropies such as symbolic dynamic entropy (SDE) [20] and permutation entropy (PE) [27] need to be improved in describing the dynamic details of the signals. In this paper, a method named ternary dynamic analysis (TDA) is proposed to extract the degradation features effectively. TDA combines the ideas of the Shannon entropy [28], local ternary pattern (LTP) [29], and optimized local ternary pattern (OLTP) [30]. State entropy (SE) and state transition entropy (STE) are obtained based on this method. The degradation state of hydraulic pumps can be identified accurately with them. The excellent effect of TDA is verified using simulated signals. The proposed method shows better performance than PE and SDE. To extract the degradation features over different scales, we develop a novel approach, which contains a method derived from an interpolation technique for the image scaling and the moving-averaging procedure, and combine it with TDA, called multi-scale ternary dynamic analysis (MTDA).

In this study, after obtaining the degradation features using MTDA, NSGA-II [31] and SVM [32] (simplified into NSGA-II-SVM) are introduced to find the most important features and recognize the different degradation states of the hydraulic pump. Moreover, the comparisons are performed among the proposed method, MMSDE-NSGA-II-SVM, and MMPE-NSGA-II-SVM. The final results show that our proposed method can obtain the highest identification accuracy with the least features. Some other studies related to the fault diagnosis of rotating machinery are also compared with our method. All the results show that our proposed method has better performance.

The following contents are also presented in this paper: the detailed procedure of the TDA method and the use of simulated signals to verify its superiority are presented in Section 2; Section 3 gives the detailed steps of MTDA; Section 4 introduces the joint optimization of feature selection and degradation state identification using NSGA-II-SVM. The process of identifying the degradation state of hydraulic pumps based on MTDA and NSGA-II-SVM proposed in this paper is illustrated in Section 5. Section 6 presents the use of experimental data to verify the effectiveness of the proposed method. The last section gives several conclusions.

2. TERNARY DYNAMIC ANALYSIS (TDA)

2.1. Details of implementing TDA

TDA is developed from LTP and OLTP, which combines the ideas of information theory. LTP and OLTP are frequently applied to the processing of grayscale images. TDA is different from them, and is used for feature extraction from vibration signals in this paper. A time series segment is reconstructed into a phase space matrix, and then the center value of each embedding vector in the matrix is compared with its neighbours. Two sets of different binary codes can be obtained based on the comparison results. The decimal form corresponding to each set of codes represents a state pattern. Then the state probability and state transition probability can be calculated. SE and STE can be obtained on this basis.

There are five steps to perform TDA based on a given signal segment $X\{x(j), j = 1,2, ..., N\}$:

1. Reconstruct the phase space based on X, and the following matrix can be obtained.

$$Z = \begin{bmatrix} Z(1) \\ Z(2) \\ Z(i) \\ \dots \\ Z(K) \end{bmatrix} =$$

$$\begin{bmatrix} x(1) & x(1+\lambda) & \dots & x(1+(m-1)\cdot\lambda) \\ x(2) & x(2+\lambda) & \dots & x(2+(m-1)\cdot\lambda) \\ x(i) & x(i+\lambda) & \dots & x(i+(m-1)\cdot\lambda) \\ \dots & \dots & \dots & \dots \\ x(K) & x(K+\lambda) & \dots & x(K+(m-1)\cdot\lambda) \end{bmatrix} \quad (1)$$

where $i = 1,2,...K$; $K = N - (m-1)\cdot\lambda$, m and λ are used to denote the embedding dimension and the time delay, respectively. It is essential to point out that m is an odd number.

2. Convert the embedding vectors $Z(i)$ into ternary patterns. In this step, P represents the number of neighbors of the center point in each row vector, and its value equals m-1. In this way, there are P/2 neighbors before and after the center point, respectively. As seen in Fig.1., an example is shown there. In this case, eight neighbors are set for the center point (Pc), including four from the left (P0, P1, P2, and P3) and four from the right (P4, P5, P6, and P7). The parameters P and σ are assigned by the user. In this example, P = 8 and σ = 0.8. In other words, m = 9 and $\beta = 0.687$. According to the following equation, the neighbor values are replaced with new values (0,1 or -1) (Fig.1.a)).

$$New\ values = \begin{cases} -1 & \text{if } p_i < (1-\sigma)p_c \\ 0 & \text{if } (1-\sigma)p_c \leq p_i \leq (1+\sigma)p_c \\ 1 & \text{if } p_i > (1+\sigma)p_c \end{cases} \quad (2)$$

where $\sigma = \beta \cdot Std$ and $i = 0, 1, \dots m-2$.
Std denotes the standard deviation of $\{P0, P1, P2...Pm-2\}$.

3. Transform the ternary patterns into two sets of binary codes, up pattern and low pattern, and compute their decimal representations, respectively. After "-1" is replaced by "0" and other values remain unchanged, the up pattern is

obtained. After "-1" is replaced by "1" and other values are all replaced by "0", the low pattern is obtained (Fig.1.b)). Subsequently, the decimal value corresponding to the binary code is calculated according to the following equation (Fig.1.c)).

$$Decimal = \sum_{n=0}^{P-1} 2^n \cdot B_i \quad (3)$$

where B_i is the value of each bit in the binary code set and equals 1 or 0. After performing the above steps, two different decimal values corresponding to each row vector of matrix Z are obtained (Fig.1.d)). For a vector with P=8, there may be 256 (2^8) decimal values. After applying these operations for each row of the matrix Z, two sets of data sequences, $S_1\{s_1(i), i = 1,2,\dots,K\}$ and $S_2\{s_2(i), i = 1,2,\dots,K\}$ are obtained, where $s_1(i)$ denotes the decimal value corresponding to $Z(i)$'s up pattern and $s_2(i)$ denotes the decimal value corresponding to $Z(i)$'s low pattern. The value of each element in the S_1 and S_2 represents a state pattern.
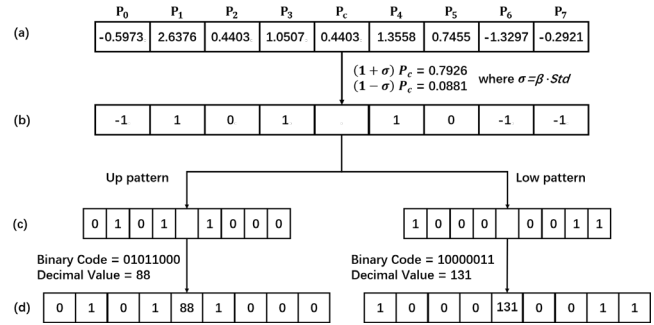

Fig.1. Steps (2) and (3) of TDA: a) the value of a row in the matrix **Z**, b) comparisons of the P_c with the P_i, c) separation of up pattern and low pattern, d) Transform the binary values into decimal form.

4. Inspired by the Shannon entropy [28], we compute the potential state patterns probability and SE based on S_1 and S_2, respectively. For example, for a given S_1, SE can be obtained by the following equation:

$$SE = -\sum_{i=1}^{A} p_i \cdot \ln p_i \quad (4)$$
$$\text{where } P_i = \frac{n_i}{N}$$

where A is the number of states. n_i is the total count of events that the i-th state occurs, N is the total count of events that all states occur. From equation (4), it can be concluded that the maximum value of SE is $\ln(2^{m-1})$ when the probability of all possible states is $1/2^{m-1}$. Then, the normalized SE by $\ln(2^{m-1})$ can be expressed as follows:

$$SE = SE/\ln(2^{m-1}) \quad (5)$$

Similarly, this step should be also applied to S_2.

5. Compute the probability of state transitions and STE. Inspired by the definition of quasi-stationary state transition probability in symbol dynamic filtering [33], we define STE as follows:

$$STE = -\sum_{i=1}^{A}\sum_{k=1}^{A} P_i \cdot P(k|i) \cdot ln[P_i \cdot P(k|i)] \quad (6)$$

$$\text{where } P(k|i) = \frac{N(i,k)}{\sum_{m=1}^{A} N(i,m)}$$

where A is the number of states. P_i is the probability of the i-th state pattern. $P(k|i)$ is the conditional probability of the k-th state, and satisfies $\sum_{k=1}^{A} P(k|i) = 1$. $N(i,k)$ is the total count of events when k-th state occurs adjacent to i-th state in the direction of motion.

The following conclusion can be drawn from equation (6): STE equals its maximum value $2 \cdot ln(2^{m-1})$ when all state pattern probabilities and state transition probabilities are $1/2^{m-1}$. Then, the normalized STE by $2 \cdot ln(2^{m-1})$ can be expressed as follows:

$$\text{STE} = \text{STE}/ [2 \cdot ln(2^{m-1})] \quad (7)$$

This step should be applied to S_1 and S_2.

After performing steps (1) to (5), four features, SE and STE of up pattern and low pattern, can be obtained based on X $\{x(j), j = 1,2, ..., N\}$.

To get a clearer and more intuitive impression, the detailed procedures of SE and STE are illustrated with the following example. For a time series X = {0.68, 0.93, 0.03, 0.88, 0.44, 0.04,1.23, 0.05, 0.98, 0.37,-1.22, -0.29, -1.81, 0.35, 1.38, -0.35, 1.79, -1.42, 0.01, -0.76}, set the parameters of the algorithm as m=9, β=0.687. After performing the steps (1) to (3) on X, two sets of data sequences are obtained: S_1 = {213, 187, 0, 220, 0, 80, 251, 230, 223, 10, 0, 58}, S_2 = {42, 0, 187, 3, 95, 174, 4, 25, 32, 117, 251, 197}. Take S_1 for example, the probability of 0 is 1/4 and marked as: P_0= 1/4. Thus the state pattern probabilities can be calculated as:

$$[P_0, P_{10}, P_{58}, P_{80}, P_{187}, P_{213}, P_{220}, P_{223}, P_{230}, P_{251}] =$$
$$\left[\frac{1}{4}, \frac{1}{12}, \frac{1}{12}, \frac{1}{12}, \frac{1}{12}, \frac{1}{12}, \frac{1}{12}, \frac{1}{12}, \frac{1}{12}, \frac{1}{12}\right] \quad (8)$$

The state transition probabilities can be calculated according to equation (6) as :

$$[P(220|0), P(80|0), \ P(58|0), P(0|10), P(251|80), P(0|187),$$
$$P(0|220), P(10|223), P(223|230), P(230|251), P(187|213)] =$$
$$\left[\frac{1}{3}, \frac{1}{3}, \frac{1}{3}, 1,1,1,1,1,1,1,1\right] \quad (9)$$

Last, calculate the SE and STE and normalize them as follows:

$$SE = -\sum_{i=1}^{A} p_i \cdot ln p_i = 2.2103 \quad (10)$$

$$SE = SE/ ln(2^{m-1}) = 0.3986 \quad (11)$$

$$STE = -\sum_{i=1}^{A}\sum_{k=1}^{A} P_i \cdot P(k|i) \cdot ln[P_i \cdot P(k|i)] = 2.2778 \quad (12)$$

$$STE = STE/ [2 \cdot ln(2^{m-1})] = 0.2054 \quad (13)$$

2.2. Comparisons among TDA, SDE, and PE

Four simulated signals are used to compare the performance of TDA, SDE and PE in measuring the complexity of the time series. In the TDA method, we only use the SE and STE of the up pattern as examples. The first three simulated signals all last for 128 seconds at a sampling frequency of 256 Hz. A sliding window with a width of 2048 sampling points and a step length of 512 sampling points is used to split the data [20]. The fourth simulated signal is 20 s with a sampling frequency of 1024 Hz. It is equally divided into ten sections, which means each section is 2 s [18].

The parameters (m, λ) of these three methods are set to the same values (5, 1) to obtain fair comparison results in this study. Meanwhile, we use the parameter β = 1.2 in the TDA method and the number of symbol ε = 10 in SDE.

The following frequency modulated (FM) signal is set to test the performance of the three methods in detecting the frequency changes of signals:

$$f_1(t) = e^{j\pi k t^2} \quad (14)$$

where the parameter k is the rate of frequency change and we set k = (5-0.1)/128 = 0.0383 here. The test results and the time-domain waveform of the FM signal are shown in Fig.2.a). We observe that the values of PE, SE, and STE generally show linear increasing trends in other periods except for short periods at the beginning. This indicates that they can describe the frequency change with higher accuracy. Compared with them, the increasing trend of SDE values is relatively insignificant and accompanied by large fluctuations.

The following amplitude modulated (AM) signal is set to investigate the performance of the three methods in detecting the amplitude changes of signals:

$$f_2(t) = e^{(-0.01t)} sin(100\pi t) \quad (15)$$

The investigation results and the time-domain waveform of the AM signal are presented in Fig.2.b). Both SE and STE values change significantly with the amplitude changes, and the SE values are more obvious, while PE values hardly change. SDE performs better than PE. The curve of SDE fluctuates to a certain extent with amplitude changes, but it is not obvious.

The following amplitude and frequency modulated (AM-FM) signal is used to study the performance of the three methods in detecting simultaneous changes in the frequency and amplitude of signals.

$$f_3(t) = 2f_1(t)sin(0.2\pi t) \quad (16)$$

As shown in Fig.2.c), the results show the excellent performance of SE and STE. Their values not only increase with the increase of frequency, but also show noticeable fluctuations with the changes of amplitude. However, PE values only increase monotonically and cannot detect the amplitude changes well. The curve of SDE shows slight fluctuations, and its increasing trend is not linear. This indicates that SDE is relatively insensitive to amplitude changes and cannot reflect linear changes of frequency.

The fourth signal shown below is used to study the performance of the three methods in describing the development process of fault for hydraulic pumps.

$$f_4(t) = x_{is}(t) + 0.06t^2 x_{fs}(t) + n(t) \qquad (17)$$
$$\text{where } x_{is}(t) = e^{-60t_1} sin(540\pi t)$$
$$x_{fs}(t) = e^{-30t_2} sin(540\pi t)$$
$$t_1 = mod(t, 1/30), \quad t_2 = mod(t, 1/6)$$

$x_{is}(t)$ simulates the inherent impact component in the vibration signal of a hydraulic pump. $x_{fs}(t)$ simulates the impact component caused by the fault of the hydraulic pump. $0.06t^2 x_{fs}(t)$ simulates the development process of fault. $n(t)$ is white noise and its intensity is -1dB here. The changing trends of the four features and the time-domain waveform of the simulated signal are shown in Fig.2.d). We can easily find that SE values and STE values show decreasing trends with the development of the fault, which are more obvious than other trends. This indicates that the TDA method can describe the degradation process of hydraulic pumps more accurately.
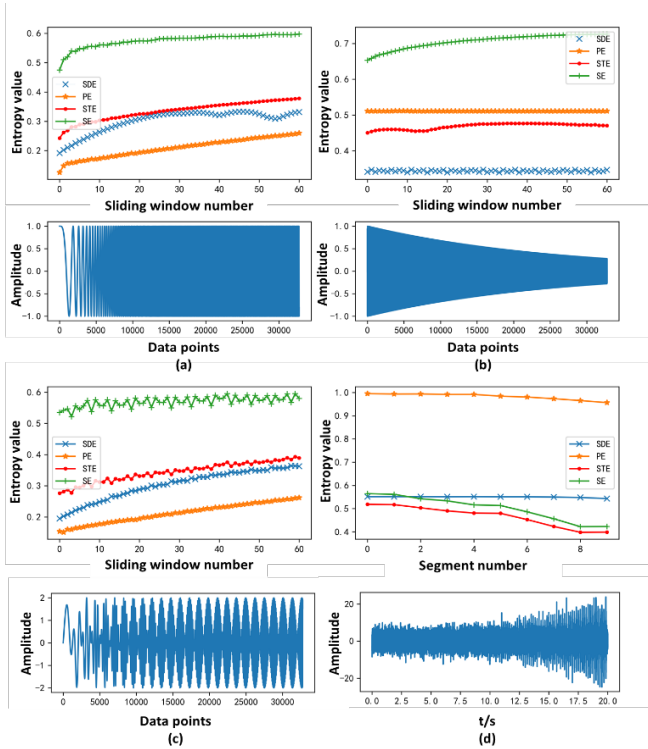

Fig.2. The simulated signals and the comparisons of TDA, PE, and SDE: a) FM signal; b) AM signal; c) AM-FM signal; d) simulated signal of the hydraulic pump degradation process.

The following conclusions can be drawn based on the above studies: (1) TDA method can accurately detect changes in signal amplitude and frequency; (2) TDA can perform well in the degradation state identification for hydraulic pumps. The reasons for the results based on the simulated signals are analyzed as: First, SDE was proposed based on PE. Naturally, the former has better performance than the latter. Second, for

a given signal sample X {x(j), j = 1,2, ..., N}, SDE converts it into a symbol series at one time, while TDA converts each embedding vector $Z(i)$ into ternary pattern, respectively. It can be seen that TDA inherits the advantages of 1D-TP as a local feature descriptor, and describes non-stationary signals more finely.

3. MULTI-SCALE TERNARY DYNAMIC ANALYSIS

3.1. Multi-scale analysis method and the process of MTDA

In this paper, a novel multi-scale analysis method is proposed, which compresses and expands the time series to extract information at different scales fully. It consists of two steps, one of which is the moving-averaging procedure [34], and the other is derived from an interpolation technique for image scaling [35]. The details of the calculation process are given below:

1. When the scale factor τ is set to different values, several new time series $\{y_j^\tau\}$ can be obtained based on a time series X {x(k), k = 1,2, ..., N} using the following equation.

$$y_j^\tau = \frac{1}{\tau}\sum_{i=j}^{j+\tau-1} x_i \qquad 1 \le j \le N - \tau + 1 \qquad (18)$$

2. When the scale factor τ' is set to different values, several new time series $\{y'_j^{\tau'}\}$ can be obtained using the following equation.

$$y'_j^{\tau'} = \{\tau' \cdot [int(\frac{j-1}{\tau'}) + 1] - j + 1\} \cdot x[int(\frac{j-1}{\tau'})] + \{j - \tau' \cdot [int(\frac{j-1}{\tau'}) + 1]\} \cdot x[int(\frac{j}{\tau'})] \qquad (19)$$
$$1 \le j \le N'$$
$$\tau' \ge 1$$

where N' represents the number of data points in the new time series, $int(\cdot)$ represents an integer operation, $x[\cdot]$ represents the value of a specified index position in the original time series. An example is used to illustrate the calculation of $y'_j^{\tau'}$ as Fig.3. In this example, the length of the original time series and that of the new time series is 4 and 6, respectively, so the scale factor τ' is 1.5. Fig.3.b) overlap values of Fig.3.a) and the new time series is computed as the percentage of overlap of the old one. It is possible to calculate the value of the new time series by weighting each value from the original time series using its overlap percentage. Thus the following equation is easy to be obtained.

$$\{y'_1^{1.5}, y'_2^{1.5}, y'_3^{1.5}, y'_4^{1.5}, y'_5^{1.5}, y'_6^{1.5}\} = \{x_1, \ 0.5 \cdot x_1 + 0.5 \cdot x_2, \ x_2, \ x_3, \ 0.5 \cdot x_3 + 0.5 \cdot x_4, \ x_4\} \qquad (20)$$

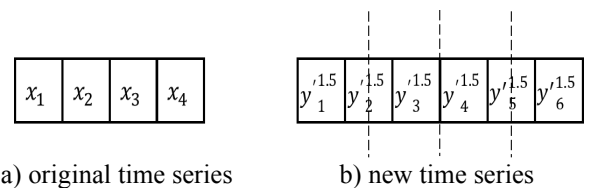a) original time series   b) new time series

Fig.3. An example to illustrate step (2) of the multi-scale analysis.

The above two steps constitute our proposed multi-scale analysis method. In particular, the original time series is expanded by performing step (2), which allows more detailed characteristics of the signal to be observed.

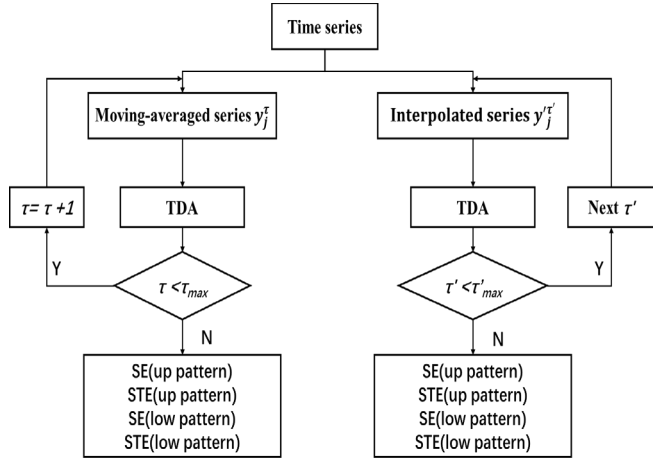The process of MTDA is shown in Fig.4.

Fig.4. The flowchart of MTDA.

3.2. DETERMINATION OF SUITABLE PARAMETERS FOR MTDA

The MTDA contains three parameters that need to be selected appropriately, including time delay λ, embedding dimension m and β. To study the influence of parameter λ, a Gaussian white noise signal with 2048 data points is used for testing. We only use the SE (up pattern), and only use the moving-averaging procedure to obtain multi-scale information. Since other situations are similar to this, they will not be shown here.

The obtained results are shown in Fig.5. The SE values decrease more significantly as the scale increases when λ = 1. There is little difference among other curves, and their

decreasing trends are relatively insignificant. Therefore, the most appropriate value of parameter λ is 1, and the SE values can be better distinguished in this case, which indicates that the algorithm can provide more sufficient information with λ = 1.

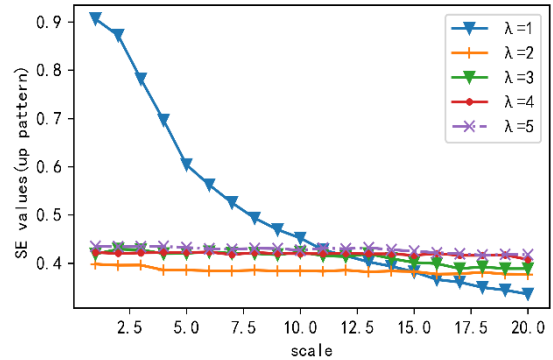Fig.5. The SE values (up pattern) of white Gaussian noise with different time delays.

To determine the optimal parameters (β, m), we tested multiple sets of values and found that the individual classification accuracy of each feature can reach a relatively high level with (β, m) = (1.6, 5). Therefore, we set the parameters (β, m) = (1.6, 5).

4. JOINT OPTIMIZATION OF FEATURE SELECTION AND DEGRADATION STATE IDENTIFICATION USING NSGA-II-SVM

After performing the above steps, a feature pool that contains amounts of information from different scales, patterns and indicators is created. However, the feature pool generally includes redundant data, which will adversely affect degradation state identification [36]. In this paper,
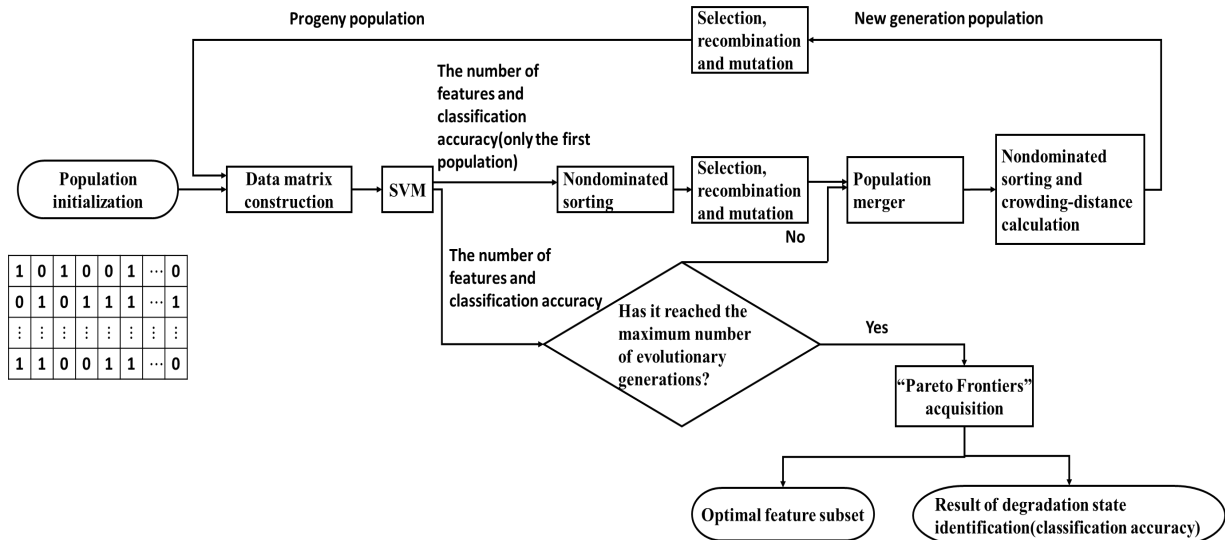

Fig.6. The flowchart of joint optimization of feature selection and degradation state identification using NSGA-II-SVM.

NSGA-II-SVM is introduced for joint optimization of feature selection and degradation state identification. NSGA-II is a multi-objective optimization genetic algorithm based on nondominated sorting. In most cases, compared with strength-Pareto EA and Pareto archive evolution strategy, it can find better convergence and solution expansion near the Pareto optimal front [31]. NSGA-II has been frequently applied in the fields of fault prognosis and diagnosis for equipment [3]-[38]. In this paper, NSGA-II is set with two objective functions: SVM classification accuracy and the total number of features fed into SVM. By setting the parameters of the algorithm, the value of the first objective function is maximized, and the value of the second one is minimized. The result of a multi-objective optimization problem is a set containing multiple optimal solutions which are called "Pareto Frontiers" [39]. In this study, the Pareto Front corresponding to the highest classification accuracy is what we need. By performing this step, the feature subset with the highest classification accuracy and the lowest dimension will be obtained. Meanwhile, the result of degradation state identification for hydraulic pumps will also be obtained. The process of joint optimization is shown in Fig.6. Note that the individual chromosome in the population takes the form of binary codes, and "1" means the corresponding feature is selected, "0" means it is not selected.

5. THE PROPOSED DEGRADATION STATE IDENTIFICATION METHOD

In this paper, a degradation state identification approach for hydraulic pumps is proposed based on MTDA and NSGA-II-SVM as follows:

1. MTDA is used to analyze the vibration signal and extract the features of the hydraulic pump under six different degradation states. We set $\beta = 1.6$, time delay $\lambda = 1$, embedding dimension $m = 5$, and two scale factors $\tau_{max} = 20$, $\tau' = (1.4, 1.5, 1.6)$;

2. NSGA-II-SVM is employed to choose the feature subset with the highest classification accuracy and identify different degradation states.

6. EXPERIMENTAL VALIDATION AND COMPARISONS

6.1. Experimental data acquisition

To verify the effectiveness of the proposed method, a hydraulic pump full life test platform was set up to collect data. The platform consists of a cooling system, a control system, signal monitoring, acquisition and display system, a pressure regulating system, and a drive system as shown in Fig.7.

The hydraulic pump used in this paper is an axial piston pump. Its parameters are as follows: type: L10VS028DFR, rated rotation speed: 1480 r/min, rated pressure: 22 MPa, displacement at the rated working condition: 28 ml/r. Three acceleration sensors are, respectively, installed in three mutually orthogonal directions as shown in Fig.8. They acquire vibration signals at a sampling frequency of 50 KHz, each sampling lasts for 1 s, and the interval between two samplings is 30 s.

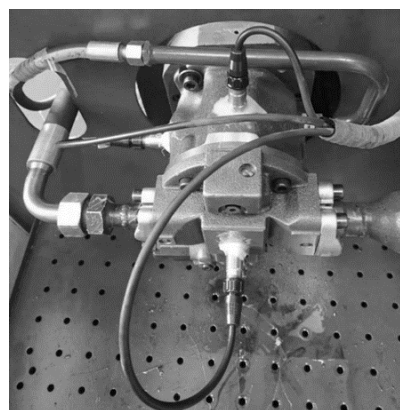Fig.7. Hydraulic pump full life test platform.

Fig.8. Layout of the three vibration sensors.

Considering that loose boot is one of the common fault pat terns of hydraulic pumps, we study the single loose boot of the hydraulic pump. The normal plungers are replaced with failed plungers obtained in the equipment maintenance to acquire more realistic vibration signals. As is presented in Fig.9., loose boot is considered under five different degrees. Vernier calliper is used to measure the longest radial distance between the plunger and the boot under the five different degrees. The measurement results defined as the loose degree are 0.12 mm, 0.18 mm, 0.3 mm, 0.42 mm, and 0.64 mm, respectively. Therefore, a total of six different degradation states, the normal state is one of them, are studied. 100 groups of vibration data in each degradation state are collected, and each group consists of 4095 data points. Some examples of vibration data are shown in Fig.10.
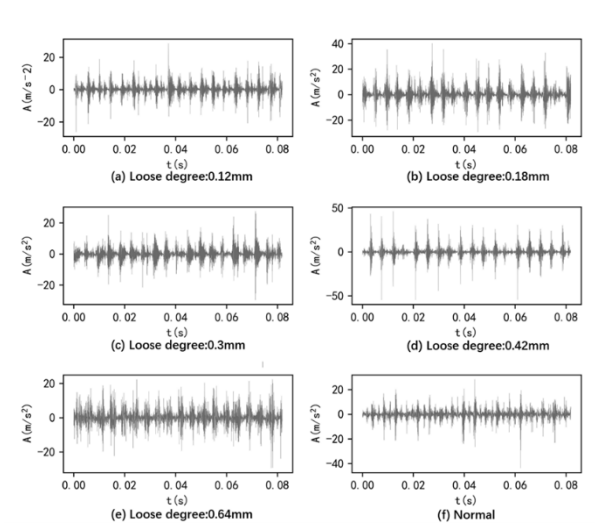

Fig.9. Loose slipper plungers.

Fig.10. Part vibration signal samples.

6.2. Comparison among MTDA, MMPE and MMSDE

The proposed method is applied to identify the six different degradation states of the hydraulic pump. First of all, MTDA is applied to obtain the features with $\tau_{max} = 20$ and $\tau' = (1.4, 1.5, 1.6)$. Second, NSGA-II-SVM is used to choose the feature subset with the highest classification accuracy and identify different degradation states. NSGA-II-SVM using MMPE (simplified into MMPE-NSGA-II-SVM) and NSGA-II-SVM using MMSDE (simplified into MMSDE-NSGA-II-SVM) are also employed to conduct the degradation state identification. Each method is implemented 15 times to reduce random effects. The highest classification accuracy and the corresponding number of features obtained in each run are shown in Fig.11. The statistical results of accuracy are shown in Table 1. The minimum number of features corresponding to the highest accuracy and the lowest accuracy is also shown in parentheses after them.

The following three conclusions can be drawn. First of all, the proposed method achieves the highest identification

accuracy (100-99.4 %). Second, it is more evident that the proposed method requires the least features (5-3) to obtain the highest identification accuracy. Third, other methods get lower identification accuracy (99.4 %-97.2 %), and it is more obvious that they require more features (7-4). Therefore, the superiority of the proposed method is reinforced.

There are three reasons for the results. First of all, MTDA combines the ideas of information theory and texture analysis technique, which makes it not only able to reflect the detailed structure of the signal, but also reflect the changes of signal complexity. Furthermore, MTDA mines rich information based on vibration signals by constructing state transition patterns and state patterns. Second, MTDA has an excellent performance in detecting frequency and amplitude changes. Third, in contrast, MMPE and MMSDE have insufficient ability to reflect signal information.

6.3. Comparison of the proposed method with previous studies

Table 2. gives some studies related to the fault diagnosis of rotating machinery, and our study is also attached to the last row. The highest classification accuracy found in each reference is recorded in the table. All methods are also tested on our hydraulic pump data to show fair comparison results. Four classifiers, Random Forest (RF), K nearest neighbor (Knn), NaiveBayes, and SVM are used.

The proposed method achieves higher accuracy than most other methods in our dataset (100 %-97.67 %). Melih's method also obtains high classification accuracy (100 %-96.17 %). However, the feature set fed to the classifier has 256 dimensions. The high-dimensional feature set may cause some trouble for subsequent operations such as feature selection and fusion, if necessary. By comparison, our feature set has only 5 dimensions. There are two reasons why the accuracy obtained by LBP is lower than that obtained by 1D-TP. One is that each data sample contains only 4095 data points, which will generate a small-size image, and the other is that 1D-TP has a stronger anti-noise capacity.
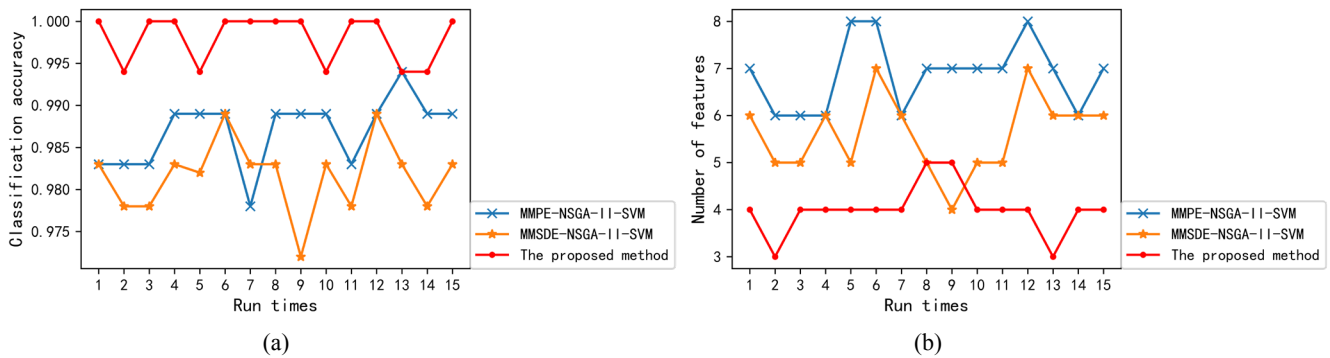

Fig.11. Comparison results of three methods using experimental signals: a) classification accuracy; b) number of features corresponding to classification accuracy.

Table 1. Degradation state identification of the three methods in the experiment.

The proposed method			MMPE-NSGA-II-SVM			MMSDE-NSGA-II-SVM		
Max	Min	Mean	Max	Min	Mean	Max	Min	Mean
1.000(4)	0.994(3)	0.998	0.994(7)	0.978(6)	0.987	0.989(7)	0.972(4)	0.981

Table 2. Comparison of the proposed method with previous studies about the rotating machinery fault.

Author(s)	Feature extraction method	Model	Dataset	Accuracy(%)			
				RF	Knn	Naive Bayes	SVM
Kaplan Kaplan et al. [26]	Local Binary Pattern (LBP[All])	Signal2Image+ LBP[All]+Classifier	Experimental setup of authors.	100	100	100	____
			Our experimental hydraulic pump data.	93.1	90.33	95	98
Melih Kuncan et al. [22]	One Dimensional Ternary Pattern (1D-TP)	Signal+1D-TP+Classifier	Experimental setup of authors.	100	100	____	100
			Our experimental hydraulic pump data.	98.8	96.17	98.67	100
Yongbo Li et al. [20]	Modified Multi-scale Symbolic Dynamic Entropy (MMSDE)	Signal+MMSDE+Minimum Redundancy Maximum Relevance (mRMR) for feature selection+Classifier	The experimental planetary gearbox data of Shandong University.	___	____	____	99.75
			Our experimental hydraulic pump data.	97	98	98.67	97.67
Jinde Zheng et al. [40]	Multi-scale Permutation Entropy (MPE)	Signal+MPE+Laplacian Score for feature selection+Classifier	Case Western Reserve University Bearing Fault Database.	____	____	____	100
			Our experimental hydraulic pump data.	92.3	86.67	89.67	96.67
Bing Han et al. [41]	Hierarchical Lempel-Ziv Complexity (HLZC)	Signal+HLZC+ Classifier	Experimental setup of authors.	___	____	____	94.72
			Our experimental hydraulic pump data.	87.6	88.67	82.33	92.3
Zhenya Wang et al. [42]	Generalized Refined Composite Multi-scale Sample Entropy (GRCMSE)	Signal+GRCMSE+Supervised Isometric Mapping(S-Isomap)+classifier	Experimental setup of authors.	___	___	___	99.72
			Our experimental hydraulic pump data.	98.63	96.06	97.96	99.78
Authors of this paper	Multi-scale Ternary Dynamic Analysis (MTDA)	Signal+MTDA+ NSGA-II-SVM	Experimental setup of authors.	97.76	97.67	98.33	100

7. SUMMARY

This paper proposes a novel method for identifying the degradation states of hydraulic pumps, which uses MTDA to extract features and uses NSGA-II and SVM to conduct feature selection and pattern recognition.

This paper has two main contributions. On the one hand,

our proposed MTDA inherits the advantages of some previous studies such as 1D-TP and SDE, which makes it more capable of describing the dynamic characteristics and complexity of non-stationary signals. Specifically, MTDA conducts ternary pattern conversion independently on the local segments of each signal sample, which is similar to 1D-

TP. Then SE and SDE are calculated to estimate the dynamical changes and complexity of each signal sample. The proposed multi-scale analysis enables MTDA to provide a more precise estimation of entropy. The effectiveness of MTDA and its superiorities in degradation feature extraction are fully validated using simulated and experimental data.

On the other hand, a novel degradation state identification scheme for hydraulic pumps based on MTDA, NSGA-II and SVM is proposed. After the feature extraction process, NSGA-II-SVM is introduced to realize the joint optimization of feature selection and pattern recognition. Due to the fast calculation, good convergence and excellent multi- objective optimization ability of NSGA-II, as well as the good classification performance of SVM, NSGA-II-SVM can find the desired feature subset and conduct high-precision pattern recognition. The superiorities of the proposed scheme in this paper are verified in Section 6. Compared with some previous studies related to the fault diagnosis of rotating machinery, it can obtain higher classification accuracy and lower feature set dimension.

However, our proposed method has a disadvantage: MTDA extracts some features that contain redundant information. For a given signal sample, four features, SE and STE of up pattern and low pattern, are acquired. From the theoretical perspective, there is a strong correlation between the up pattern and the low pattern. Although we alleviate this disadvantage through feature selection, there are other better methods worth exploring.

In our future work, we plan to address this disadvantage in two ways. One is to learn from more advanced texture descriptors to avoid deriving two patterns from the same signal, and the other is to study an effective algorithm to fuse the extracted features.

REFERENCES

[1] Zheng, Z., Wang, Z., Zhu, Y., Tang, S., Wang, B. (2019). Feature extraction method for hydraulic pump fault signal based on improved empirical wavelet transform. *Processes*, 7 (11), 824.

[2] Wang, X., Lin, S., Wang, S., He, Z., Zhang, C. (2016). Remaining useful life prediction based on the Wiener process for an aviation axial piston pump. *Chinese Journal of Aeronautics*, 29 (3), 779-788.

[3] Doa'Ei, Y., Jahan, A.M. (2018). Application of articial intelligence and meta-heuristic algorithms in civil health monitoring systems. *Civil Engineering Journal*, 4 (7), 1653-1666.

[4] Lu, C., Wang, S., Wang, X. (2017). A multi-source information fusion fault diagnosis for aviation hydraulic pump based on the new evidence similarity distance. *Aerospace Science and Technology*, 71, 392-401.

[5] Cernetic, J. (2009). The use of noise and vibration signals for detecting cavitation in kinetic pumps. *Proceedings of the Institution of Mechanical Engineers, Part C: Journal of Mechanical Engineering Science*, 223 (7), 1645-1655.

[6] Sun, J., Li, H., Xu, B. (2016). The morphological undecimated wavelet decomposition–discrete cosine transform composite spectrum fusion algorithm and its application on hydraulic pumps. *Measurement*, 94, 794-805.

[7] Zhong, K., Han, M., Han, B. (2019). Data-driven based fault prognosis for industrial systems: A concise overview. *IEEE/CAA Journal of Automatica Sinica*, 7 (2), 330-345.

[8] Dong, S., Tang, B., Chen, R. (2013). Bearing running state recognition based on non-extensive wavelet feature scale entropy and support vector machine. *Measurement*, 46 (10), 4189-4199.

[9] Tahir, M.M., Khan, A.Q., Iqbal, N., Hussain, A., Badshah, S. (2016). Enhancing fault classification accuracy of ball bearing using central tendency based time domain features. *IEEE Access*, 5, 72-83.

[10] Wang, Z., Zhang, Q., Xiong, J., Xiao, M., Sun, G., He, J. (2017). Fault diagnosis of a rolling bearing using wavelet packet denoising and random for-ests. *IEEE Sensors Journal*, 17 (17), 5581-5588.

[11] Xu, Y., Tian, W., Zhang, K., Ma, C. (2019). Application of an enhanced fast kurtogram based on empirical wavelet transform for bearing fault diagnosis. *Measurement Science and Technology*, 30 (3), 035001.

[12] Yan, X., Jia, M. (2018). A novel optimized SVM classification algorithm with multi-domain feature and its application to fault diagnosis of rolling bearing. *Neurocomputing*, 313, 47-64.

[13] Dai, J., Tang, J., Huang, S., Wang, Y. (2019). Signal-based intelligent hydraulic fault diagnosis methods: Review and prospects. *Chinese Journal of Mechanical Engineering*, 32(1), 75.

[14] Li, H., Tian, Z., Yu, H., Xu, B. (2019). Fault prognosis of hydraulic pump based on bispectrum entropy and deep belief network. *Measurement Science Review*, 19 (5), 195-203.

[15] Marinoni, A., Gamba, P. (2017). Unsupervised data driven feature extraction by means of mutual information maximization. *IEEE Transactions on Computational Imaging*, 3 (2), 243-253.

[16] Ray, A. (2004). Symbolic dynamic analysis of complex systems for anomaly detection. *Signal Processing*, 84 (7), 1115-1130.

[17] Kaya, Y., Ertugrul, O.F. (2016). A novel feature extraction approach in SMS spam filtering for mobile communication: One-dimensional ternary patterns. *Security and Communication Networks,* 9 (17), 4680-4690.

[18] Wang, Y., Li, H., Wang, B., Xu, B. (2015). Spatial information entropy and its application in the degradation state identification of hydraulic pump. *Mathematical Problems in Engineering*, 7, 1-11.

[19] Wu, Z., Jiang, H., Zhao, K., Li, X. (2019). An adaptive deep transfer learning method for bearing fault diagnosis. *Measurement*, 151, 107227.

[20] Li, Y., Yang, Y., Li, G., Xu, M., Huang, W. (2017). A fault diagnosis scheme for planetary gearboxes using modified multi-scale symbolic dynamic entropy and mRMR feature selection. *Mechanical Systems and Signal Processing*, 91, 295-312.

[21] Ruiz, M., Mujica, L.E., Alferez, S., Acho, L., Tutiven, C., Vida, Y., Rodellar, J., Pozo, F. (2018). Wind turbine fault detection and classification by means of image texture analysis. *Mechanical Systems and Signal Processing*, 107, 149-167.

[22] Kuncan, M., Kaplan, K., Minaz, M.R., Kaya, Y., Ertunc, H.M. (2020). A novel feature extraction method for bearing fault classification with one dimensional ternary patterns. *ISA Transactions*, 100, 346-357.

[23] Kaya, Y., Kuncan, M., Kaplan, K., Minaz, M.R., Ertunc, H.M. (2021). A new feature extraction approach based on one dimensional gray level co-occurrence matrices for bearing fault classification. *Journal of Experimental & Theoretical Artificial Intelligence*, 33 (1), 161-178.

[24] Kaya, Y., Kuncan, M., Kaplan, K., Minaz, M.R., Ertunc, H.M. (2020). Classification of bearing vibration speeds under 1D-LBP based on eight local directional filters. *Soft Computing*, 24 (16), 12175-12186.

[25] Kuncan, M. (2020). An intelligent approach for bearing fault diagnosis: Combination of 1D-LBP and GRA. *IEEE Access*, 8, 137517-137529.

[26] Kaplan, K., Kaya, Y., Kuncan, M., Minaz, M.R., Ertunc, H.M. (2020). An improved feature extraction method using texture analysis with LBP for bearing fault diagnosis. *Applied Soft Computing*, 87, 106019.

[27] Bandt, C., Pompe, B. (2002). Permutation entropy: A natural complexity measure for time series. *Physical Review Letters*, 88 (17), 174102.

[28] Shannon, C.E. (2001). A mathematical theory of communication. *Mobile Computing and Communications Review*, 5 (1), 3-55.

[29] Reddy, K.S., Kumar, V.V., Reddy, B.E. (2015). Face recognition based on texture features using local ternary patterns. *International Journal of Image, Graphics & Signal Processing*, 7 (10).

[30] Raja, M., Sadasivam, V. (2013). Optimized local ternary patterns: A new texture model with set of optimal patterns for texture analysis. *Journal of Computer Science*, 9 (1), 1-15.

[31] Deb, K., Pratap, A., Agarwal, S., Meyarivan, T. (2002). A fast and elitist multiobjective genetic algorithm: NSGA-II. *IEEE Transactions on Evolutionary Computation*, 6 (2), 182-197.

[32] Noble, W.S. (2006). What is a support vector machine? *Nature Biotechnology*, 24 (12), 1565-1567.

[33] Li, Y., Xu, M., Wei, Y., Huang, W. (2016). Health condition monitoring and early fault diagnosis of bearings using SDF and intrinsic characteristic-scale decomposition. *IEEE Transactions on Instrumentation and Measurement,* 65 (9) 2174-2189.

[34] Wu, S.D., Wua, C.W., Lee, K.Y., Lin, S.G. (2013). Modified multiscale entropy for short-term time series analysis. *Physica A*, 392 (23), 5865-5873.

[35] Prasantha, H.S. (2020). Novel approach for image scaling using interpolation techniques. *International Journal of Creative Research Thoughts*, 8 (8), 1856-1861.

[36] Hu, Q., Si, X.-S., Qin, A.-S., Lv, Y.-R., Zhang, Q.-H. (2020). Machinery fault diagnosis scheme using redefined dimensionless indicators and mRMR feature selection. *IEEE Access*, 8, 40313-40326.

[37] Wang, S., Zhao, D., Yuan, J., Li, H., Gao, Y. (2019). Application of NSGA-II Algorithm for fault diagnosis in power system. *Electric Power Systems Research*, 175, 105893.

[38] Arjmand-M, A.H., Sargolzaei, N. (2016). Intelligent fault diagnosis of induction motors based on multi-objective feature selection using NSGA-II. In *2016 6th International Conference on Computer and Knowledge Engineering (ICCKE)*. IEEE, 183-188.

[39] Kim, I.Y., De Weck, O.L. (2005). Adaptive weighted-sum method for bi-objective optimization: Pareto front generation. *Structural and Multidisciplinary Optimization*, 29 (2), 149-158.

[40] Zheng, J., Cheng, J., Yang, Y. (2014). Multiscale permutation entropy based rolling bearing fault diagnosis. *Shock and Vibration*, 1, 1-8.

[41] Han, B., Wang, S., Zhu, Q., Yang, X., Li, Y. (2020). Intelligent fault diagnosis of rotating machinery using hierarchical Lempel-Ziv complexity. *Applied Sciences*, 10 (12), 4221.

[42] Wang, Z., Yao, L., Cai, Y. (2020). Rolling bearing fault diagnosis using generalized refined composite multiscale sample entropy and optimized support vector machine. *Measurement*, 156, 107574.